

**CrystEngComm****Suppressing Barite Crystallization with Organophosphorus Compounds**

Journal:	<i>CrystEngComm</i>
Manuscript ID	CE-ART-06-2021-000813.R1
Article Type:	Paper
Date Submitted by the Author:	17-Sep-2021
Complete List of Authors:	Sosa, Ricardo; University of Houston, Conrad, Jacinta; University of Houston, Reynolds, Michael; Shell Upstream Americas, Completions and Technology Effectiveness Rimer, Jeffrey; University of Houston, Chemical and Biomolecular Engineering

SCHOLARONE™
Manuscripts

PAPER

Suppressing Barite Crystallization with Organophosphorus Compounds

Ricardo D. Sosa,^a Jacinta C. Conrad,^a Michael A. Reynolds,^b and Jeffrey D. Rimer*^a

Received 00th January 20xx,
Accepted 00th January 20xx

DOI: 10.1039/x0xx00000x

Molecular modifiers can display a wide range of interactions with crystal interfaces to impede their growth. In this work we evaluate the efficacy of a naturally derived phosphorous-containing molecule, phytate, as an inhibitor of barite crystallization compared to the performance of a commercial organophosphorus standard. We show that both compounds inhibit barite nucleation and growth, with phytate demonstrating enhanced potency over the benchmark compound. Our findings reveal that phytate operates by a distinct mode of action on multiple crystal facets, imparting exceptional efficacy, which combined with its biocompatibility and widespread availability make phytate a potentially viable environmentally-friendly alternative to current barite scale treatments.

Introduction

Mineralization of common inorganic components can have a detrimental impact on processes ranging from water purification and energy production¹⁻⁴ to pathological diseases.⁵⁻⁹ Among the more problematic minerals in commercial processes is barium sulfate (barite), a sparingly soluble component with few chemical treatment options available to suppress scale formation. Typically, the use of compounds such as diethylenetriamine pentamethylenephosphonic acid (DTPMP) and other analogues are implemented in scale prevention formulations.¹⁰⁻¹² These molecular additives are efficient inhibitors of barite crystallization owing to their abundance of strong phosphonate acid groups ($-\text{PO}_3^{2-}$), which exhibit a specificity for binding to barite crystal facets and impeding growth. Identification of effective modifiers has spurred significant interest in understanding their interaction with crystal surfaces and mode of action to inhibit barite scale,¹³⁻¹⁹ among a broader range of minerals.²⁰⁻²¹ An essential component of modifier design is the identification of molecules with proximal acid groups,²² which can act cooperatively as binding moieties that enable modifier adsorption on crystal surfaces to frustrate the incorporation of growth units (i.e. solute).

In this study, we examined the efficacy and mechanism of phytic acid (or *myo*-phytate) as a naturally derived molecular inhibitor of barite crystallization. Phytate used in this study is a bio-derivative of the naturally occurring sugar molecule, cis-

1,2,3,5-trans-4,6-cyclohexanehexol (i.e. *myo*-inositol), in which the alcohol groups have been substituted by six phosphate groups to form the phosphate ester.²³ This *myo*-phytate isomer has been widely investigated for its application in the food industry due to its ability to chelate alkaline earth metals (e.g. Ca^{2+} ions) and in forming insoluble polyphosphate – ion complexes.²⁴⁻²⁹ The efficiency of phytate as a chelating agent and its use in commercial scale inhibitor formulations³⁰ motivated our investigation of its potential to act as a crystal growth inhibitor.³¹⁻³⁶ Herein we compare the efficacy of phytate to that of a benchmark phosphonate, DTPMP. It should be noted that organo-phosphonic acids such as DTPMP and organo-phosphoric acids such as phytic acid are different classes of molecules. For instance, DTPMP is an organo-phosphonic acid that is effective at both high pH (9.5 – 12) and temperature ($> 210\text{ }^\circ\text{C}$), whereas phytates are organo-phosphate esters of phytic acid that are known to decompose at lower temperatures ($150\text{ }^\circ\text{C}$).³⁷ Using a combination of microfluidics and scanning probe microscopy, we confirmed that both modifiers exhibit dual characteristics as nucleation and growth inhibitors, with phytate being a more potent and potentially more environmentally friendly alternative to commercial analogues.

Results and Discussion

We assessed the efficacy of *myo*-phytate (PA) as an inhibitor of barite crystallization using the commercial scale inhibitor DTPMP as a benchmark. DTPMP is a polyamine decorated with five phosphonic acid substituents (Fig. 1A) and 10 protons with acid dissociation constants (pK_a) spanning 1.04 to 12.58.³⁸ Full deprotonation of DTPMP is achieved under severely caustic conditions; however, prior studies have shown that DTPMP is a highly effective inhibitor of barite crystallization in its partially dissociated state (i.e. maximum of six dissociated hydrogens)

^a Department of Chemical and Biomolecular Engineering, University of Houston, Houston, Texas 77204, United States

^b Shell Exploration and Production Company, Houston, TX 77079, USA

† Electronic Supplementary Information (ESI) available: Experimental methods, additional micrographs and data analysis from bulk crystallization and microfluidics assays, images and data analysis from OIM measurements, movie captions. See DOI: 10.1039/x0xx00000x

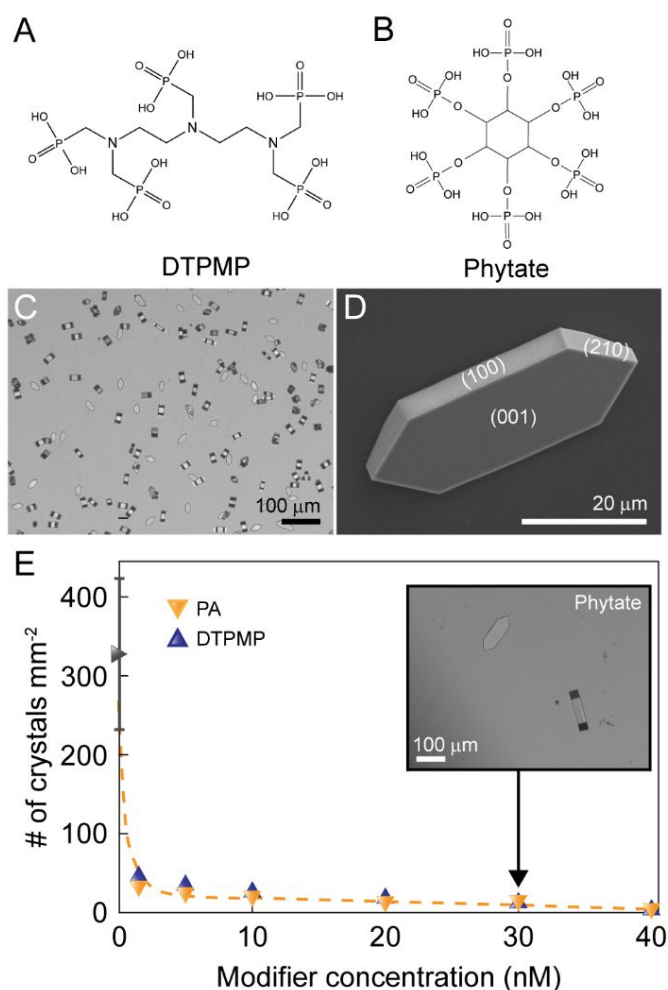


Fig. 1. Molecular structures of (A) DTPMP and (B) phytate. (C) Representative optical micrograph of barite crystals synthesized in bulk assays under quiescent conditions using a supersaturated solution ($S = 10$) at room temperature (24 h period). (D) Scanning electron image of a barite crystal with indexed facets. (E) Number density of crystals at the bottom of glass synthesis vials as a function of modifier concentration. Inset: representative micrograph of the crystal population in the presence of phytate (see Fig. S4† for an image with DTPMP). Symbols are the average of 30 measurements for 3 experiments. Error bars span two standard deviations (those not shown are smaller than the symbol). Dashed lines are interpolated to guide the eye.

around neutral pH.³⁹⁻⁴⁰ In comparison, PA is slightly more negatively charged at neutral pH with seven dissociated hydrogens.⁴¹ Notably, PA contains 12 hydrogens capable of dissociation (Fig. 1B) where the first four to dissociate are strong acids ($pK_a \sim 2$) and the last 4 protons to dissociate are weak acids that require strongly caustic conditions ($pH > 10$) to achieve full deprotonation. Typical operating conditions ($pH 2 - 10$) for processes involving barite scale formation would lead to three dominant phytate species: PA^{6-} , PA^{7-} , and PA^{8-} .⁴¹ The presence of multiple (and proximal) acids enables both PA and DTPMP to sequester free barium ions in solution, as well as bind to barite crystal surfaces through facet-specific modifier-crystal interactions.

In bulk crystallization assays, barite was synthesized under quiescent conditions using a growth solution with a supersaturation ratio of $S = 10$. This condition yields a large number density of crystals (340 ± 90 crystals mm^{-2}), which was

quantified by counting the number of crystals that sediment to the bottom of glass vials per unit area. Barite crystals prepared in this way exhibited an elongated hexagonal platelet morphology (Fig. 1C) with three dominant facets: basal (001), apical (210), and side (100) surfaces (Fig. 1D). Bulk crystallization assays in the presence of PA and DTPMP showed a sharp decline in crystal number density (Fig. 1E) with increasing modifier concentration. Within 24 h of preparing the growth solution, we observed complete suppression of barite nucleation at low modifier concentration (ca. 50 nM) with no difference in the trends for PA and DTPMP. As expected, a lower nucleation rate leads to fewer crystals that are larger in size (inset of Fig. 1E), with no appreciable difference in crystal aspect ratio (Fig. S1 and S2†). Extending the exposure time to 14 days using 50 nM modifier revealed only a single crystal with [010] length greater than 500 μm (Fig. S3†).

It could be surmised that modifier suppression of barite nucleation involves the inhibition of clusters (precursors) if the process involves a nonclassical two-step mechanism,⁴²⁻⁴⁵ as suggested in prior literature for barium sulfate solutions containing polymeric additives.⁴⁶⁻⁴⁷ To test for this possibility, we performed oblique illumination microscopy (OIM), which is a scattering technique used to characterize particles by Brownian dynamics.⁴⁸⁻⁴⁹ Solutions prepared at saturation ($S = 1$) did not show any evidence of clusters over a 3-day period (Fig. S5†), suggesting nucleation occurs via a classical pathway.^{45, 50} Similar experiments were performed in a supersaturated solution ($S = 10$) with various concentrations of each modifier (10–50 nM). OIM measurements of these solutions after initial mixing of reagents (ca. 30 s) revealed particles with sizes spanning from 30 to 200 nm (Fig. S6 and Movie S1†). Our findings revealed that the population of particles decreased with increasing modifier concentration, such that the highest concentration tested (50 nM) completely suppressed nucleation (Fig. S7†), consistent with observations in bulk crystallization assays (Fig. 1E).

In a previously published study we identified certain modifiers (e.g. alginate) with a dual capability of inhibiting barite nucleation and growth.⁵¹ Here we also observed dual inhibitory behavior for both PA and DTPMP. Studies of crystal growth inhibition were performed using a combination of microfluidics and *in situ* atomic force microscopy (AFM). Using a microfluidic setup adapted from a previous study,⁵² microchannels were seeded with barite crystals and growth solutions with or without modifier were continuously supplied ($12 mL h^{-1}$) to maintain a constant supersaturation ($S = 7$) slightly less than that of bulk crystallization assays to prevent homogenous nucleation. The growth solutions supplied to the microfluidic device for seeded growth studies were thoroughly mixed prior to injection into the microchannels, as described in detail in our previous study⁵² where we systematically assessed the effect of flow on the growth of barite in the presence and absence of modifiers. Here, time-resolved images (Fig. 2A and Movie S2†) showed significant inhibition of barite growth at 40 nM PA with noticeable changes in crystal habit, i.e. a blunting of apical tips to generate new (010) facets and a reduction in the length-to-width aspect ratio (or [010]/[100] dimensions).

Microfluidic measurements revealed complete suppression of growth once the concentration of PA (or DTPMP) reached 50 nM, which is identical to the concentration required to suppress nucleation. The inhibition of barite growth is evident in Fig. 2B by the monotonic reduction in relative growth rate with increasing

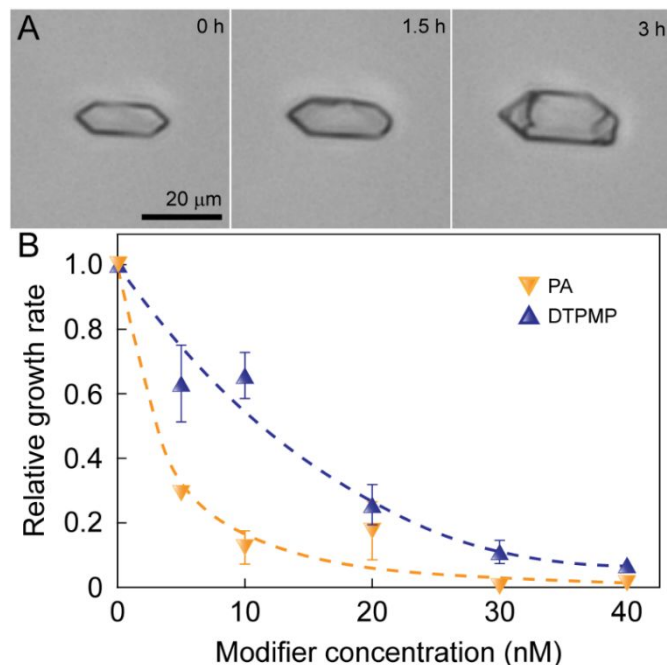


Fig. 2. *In situ* microfluidic assays in the presence of DTPMP and phytate. (A) Time-resolved optical images of a crystal growing in a supersaturated solution ($S = 7$) containing 40 nM phytate at room temperature. (B) Relative growth rate of barite crystal (001) surface area exposed to flowing aqueous solutions of phytate and DTPMP as a function of modifier concentration. Symbols represent the average of more than 100 crystals. Error bars span two standard deviations (those not shown are smaller than the symbol). Dashed lines are interpolated to guide the eye.

modifier concentration. Growth inhibition is primarily attributed to modifier interactions with barite crystal surfaces rather than modifier sequestration of Ba^{2+} ions, which requires comparable concentrations of both modifier and solute to appreciably reduce supersaturation. Indeed, the nearly 10^3 differences in solute (0.5 mM) and modifier (0.5 μM) concentration suggests PA and DTPMP inhibit barite growth via a kinetic mechanism. We report the relative growth rate as the temporal change in (001) surface area in the presence of modifier scaled by its value in the absence of modifier. Comparison of PA and DTPMP shows that the former is a more potent growth inhibitor (i.e. suppression of barite crystallization occurs at much lower PA concentration).

We conducted *in situ* AFM measurements to glean microscopic insight on the growth mechanisms of barite under flow and in the presence of PA. In a previous study⁵¹ we confirmed that barite surfaces in the absence of modifier grow by 2-dimensional layer generation and spreading to yield surfaces with triangular-shaped islands. Here we used *in situ* AFM to show that islands on barite (001) surfaces undergo a

geometrical transition from triangular to rounded islands in the presence of PA (Fig. 3A). Time-resolved images extracted from Movie S3† reveal that PA significantly reduces the rate of step advancement, thereby creating fixed terrace surface area for island nucleation. Over the course of continuous imaging we observed an increased density of 2D islands populating the surface; however, the presence of PA prevents further growth of newly generated layers, leading to a rough surface where island generation and spreading are both fully suppressed after 15 min.

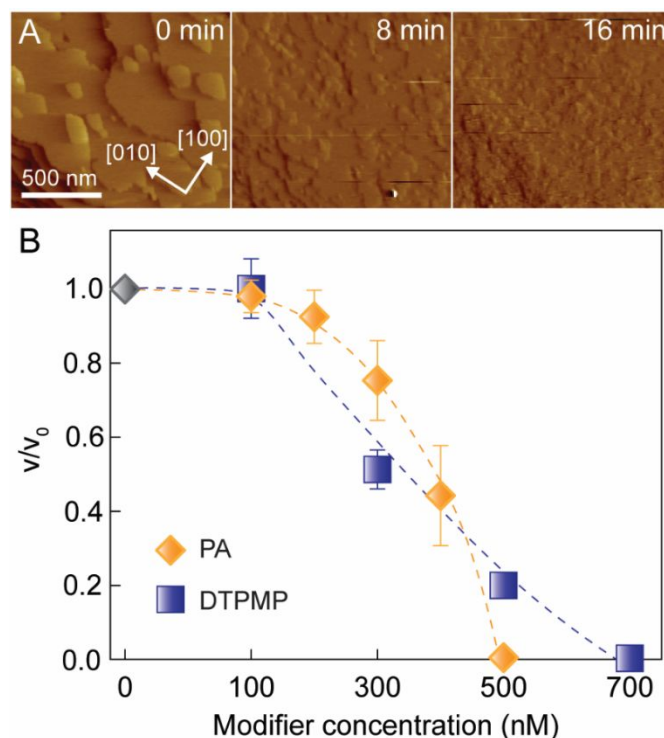


Fig. 3. (A) Temporal images from *in situ* AFM showing suppressed growth of a barite (001) surface after exposure to a supersaturated solution ($S = 7$) containing 500 nM phytate. (B) Relative step velocities of 2D layers measured in the [010] direction in the presence of phytate (yellow diamonds) and DTPMP (blue squares). Symbols represent an average of 60 islands measured in the absence and presence of modifier to calculate v and v_0 , respectively. Error bars span two standard deviations, where those not visible are smaller than the symbol. Dashed lines are interpolated to guide the eye.

Sequential AFM images were used to measure temporal advancement of layers in the [010] direction. From this data we extracted step velocity (v) in the presence of modifier, which was scaled by its value v_0 in the absence of modifier. The monotonic reduction in v/v_0 to zero with increasing modifier concentration (Fig. 3B) indicates a step pinning mechanism of surface growth inhibition.⁵³⁻⁵⁴ Comparison of step velocity profiles for PA and DTPMP reveals a sharp decrease in relative step velocities of 2D layers in the presence of PA, whereas increasing DTPMP concentration results in a non-parabolic monotonic decrease in step velocity. The velocity of layer advancement on basal surfaces impacts out-of-plane growth (c -direction), which is difficult to assess by AFM owing to the

challenge of mounting crystals with (100) surfaces oriented normal to the plane of imaging. In contrast, seeding of microchannels results in a small population of α -oriented crystals (Fig. S8†) for which time-resolved imaging by microfluidics shows growth along the [001] direction at concentrations where growth along both b - and a -directions are fully suppressed. These observations indicate PA and DTPMP are more potent inhibitors of growth along [100] and [010] directions (i.e. which exhibit the fastest rates of growth in barite crystals); a desirable outcome from the standpoint of optimizing anti-scaling agents.

The ability to seed microchannels with different barite crystal orientations relative to the viewing area enables analysis of growth and its inhibition along all principal crystallization directions.⁵² Similar crystal orientations are achieved in AFM sample preparation; however, measurements of barite (100) surface growth reveal topographies devoid of distinct layers (Fig. 4A), which makes *in situ* analysis of step velocity impossible. Interestingly, distinct features appear on barite (100) surfaces in solutions containing PA but not in identical experiments with DTPMP. The presence of PA generates

understood, nor is its relation (if any) to the enhanced efficacy of PA over DTPMP as an inhibitor of barite crystallization. To our knowledge, hillocks on barite (100) surfaces are not observed in previous studies.

Conclusions

In summary, we have shown that phytate functions as a dual action inhibitor of barite nucleation and crystal growth. At nanomolar concentrations of both phytate and DTPMP, we observed complete suppression of barite nucleation. Microfluidic studies of barite crystal growth revealed that phytate suppresses crystallization at concentrations nearly one-third those of DTPMP (Fig. 2B), indicating phytate is a more potent growth inhibitor. Time-resolved atomic force microscopy revealed that both phytate and DTPMP operate by an efficient step pinning mode of action, which fully suppresses layer nucleation and advancement. Given that phytate is a natural compound derived from food sources (e.g. grains and nuts), it has potential as a green alternative to commercial scale treatments, such as DTPMP.

Conflicts of interest

There are no conflicts to declare.

Acknowledgements

We wish to thank Dipayan Chakraborty for assistance with *in situ* AFM measurements and Dr. Xi Geng for useful discussions. We acknowledge financial support from Shell Oil Company and the National Science Foundation Graduate Student Fellowship (Award DGE 1144207). JDR and JCC also acknowledge support from the Welch Foundation (Awards E-1794 and E-1869, respectively).

References

1. Reynolds, M. A., A Technical Playbook for Chemicals and Additives Used in the Hydraulic Fracturing of Shales. *Energy & Fuels* **2020**, *34* (12), 15106-15125.
2. Mpelwa, M.; Tang, S.-F., State of the art of synthetic threshold scale inhibitors for mineral scaling in the petroleum industry: a review. *Petroleum Science* **2019**, *16* (4), 830-849.
3. García, A. V.; Thomsen, K.; Stenby, E. H., Prediction of mineral scale formation in geothermal and oilfield operations using the extended UNIQUAC model: Part I. Sulfate scaling minerals. *Geothermics* **2005**, *34* (1), 61-97.
4. Bellarby, J., Chapter 7 Production Chemistry. In *Developments in Petroleum Science*, Bellarby, J., Ed. Elsevier: 2009; Vol. 56, pp 371-432.
5. Olafson, K. N.; Nguyen, T. Q.; Rimer, J. D.; Vekilov, P. G., Antimalarials inhibit hemozoin crystallization by unique drug-surface site interactions. *Proceedings of the National Academy of Sciences* **2017**, *114* (29), 7531-7536.
6. Olafson, K. N.; Ketchum, M. A.; Rimer, J. D.; Vekilov, P. G., Mechanisms of hemozoin crystallization and inhibition by the

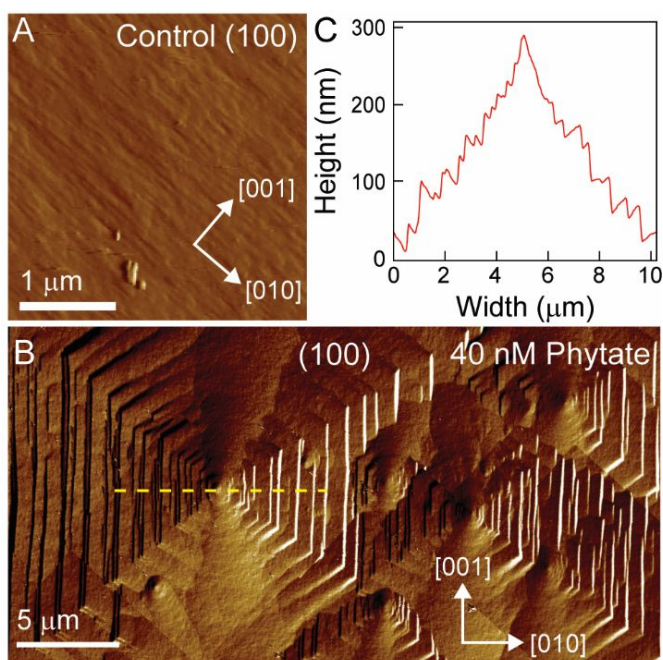


Fig. 4. (A) *Ex situ* AFM image of a barite (100) surface on a crystal grown in supersaturated solution ($S = 10$) without modifier (control). (B) Tile-stitched *ex situ* images of multiple areas on a barite (100) surface for a crystal grown in 40 nM phytate. The surface contains large macrosteps arranged in the form of hillocks. (C) Height profile of a macrostep hillock measured along the yellow dashed line in panel B.

pyramidal macrosteps where edges along the [001] direction are less defined, leading to an asymmetric surface topography (Fig. 4B). A representative height profile measured along one of the pyramids (Fig. 4C) shows that steps vary in height with sizes well exceeding single layers (i.e. macrosteps comprising more than 1000 unit cells). The exact mechanism by which PA generates pyramidal features on (100) surfaces is not well

- antimalarial drug chloroquine. *Proceedings of the National Academy of Sciences* **2015**, *112* (16), 4946-4951.
7. Ma, W.; Lutsko, J. F.; Rimer, J. D.; Vekilov, P. G., Antagonistic cooperativity between crystal growth modifiers. *Nature* **2020**, *577* (7791), 497-501.
 8. Kim, D.; Olympiou, C.; McCoy, C. P.; Irwin, N. J.; Rimer, J. D., Time-Resolved Dynamics of Struvite Crystallization: Insights from the Macroscopic to Molecular Scale. *Chemistry-A European Journal* **2020**, *26* (16), 3555-3563.
 9. Kim, D.; Moore, J.; McCoy, C. P.; Irwin, N. J.; Rimer, J. D., Engaging a Battle on Two Fronts: Dual Role of Polyphosphates as Potent Inhibitors of Struvite Nucleation and Crystal Growth. *Chemistry of Materials* **2020**, *32* (19), 8672-8682.
 10. Powell, P.; Singleton, M. A.; Sorbie, K. S. Combined scale inhibitor and water control treatments. **2005**, US Patent 6,913,081.
 11. Frenier, W.; Ziauddin, M.; Davies, S.; Chang, F. Composition and method for treating a subterranean formation. **2007**, US Patent 7,192,908.
 12. Faugerstrom, L.; Horton, R. L.; Luyster, M.; Shepherd, C.; Prasek, B. B.; Lepage, J. Chelate Compositions And Methods And Fluids For Use In Oilfield Operations. **2014**, US Patent 20140151042 .
 13. Pina, C. M.; Putnis, C. V.; Becker, U.; Biswas, S.; Carroll, E. C.; Bosbach, D.; Putnis, A., An atomic force microscopy and molecular simulations study of the inhibition of barite growth by phosphonates. *Surface Science* **2004**, *553* (1), 61-74.
 14. Mavredaki, E.; Neville, A.; Sorbie, K. S., Initial stages of barium sulfate formation at surfaces in the presence of inhibitors. *Crystal Growth & Design* **2011**, *11* (11), 4751-4758.
 15. Leung, W. H.; Nancollas, G. H., A kinetic study of the seeded growth of barium sulfate in the presence of additives. *Journal of Inorganic and Nuclear Chemistry* **1978**, *40* (11), 1871-1875.
 16. Jones, F.; Oliveira, A.; Rohl, A.; Parkinson, G.; Ogden, M.; Reyhani, M., Investigation into the effect of phosphonate inhibitors on barium sulfate precipitation. *Journal of Crystal Growth* **2002**, *237*, 424-429.
 17. Jones, F.; Jones, P.; De Marco, R.; Pejcic, B.; Rohl, A. L., Understanding barium sulfate precipitation onto stainless steel. *Applied Surface Science* **2008**, *254* (11), 3459-3468.
 18. Bukuaghain, O.; Neville, A.; Charpentier, T. In *Scale Formation in Multiphase Conditions*, Proceedings of the Oil Field Chemistry Symposium, Gielo, **2015**.
 19. Black, S. N.; Bromley, L. A.; Cottier, D.; Davey, R. J.; Dobbs, B.; Rout, J. E., Interactions at the organic/inorganic interface: binding motifs for phosphonates at the surface of barite crystals. *Journal of the Chemical Society, Faraday Transactions* **1991**, *87* (20), 3409-3414.
 20. Zieba, A.; Sethuraman, G.; Perez, F.; Nancollas, G. H.; Cameron, D., Influence of Organic Phosphonates on Hydroxyapatite Crystal Growth Kinetics. *Langmuir* **1996**, *12* (11), 2853-2858.
 21. Jarrahian, K.; Sorbie, K. S., Mechanistic Investigation of Adsorption Behavior of Two Scale Inhibitors on Carbonate Formations for Application in Squeeze Treatments. *Energy & Fuels* **2020**, *34* (4), 4484-4496.
 22. Olafson, K. N.; Li, R.; Alamani, B. G.; Rimer, J. D., Engineering Crystal Modifiers: Bridging Classical and Nonclassical Crystallization. *Chemistry of Materials* **2016**, *28* (23), 8453-8465.
 23. Loewus, F. A.; Murthy, P. P. N., myo-Inositol metabolism in plants. *Plant Science* **2000**, *150* (1), 1-19.
 24. Zhou, J. R.; Erdman, J. W., Phytic acid in health and disease. *Critical Reviews in Food Science and Nutrition* **1995**, *35* (6), 495-508.
 25. Oatway, L.; Vasanthan, T.; Helm, J. H., PHYTIC ACID. *Food Reviews International* **2001**, *17* (4), 419-431.
 26. Liang, J.; Han, B.-Z.; Nout, M. J. R.; Hamer, R. J., Effect of soaking and phytase treatment on phytic acid, calcium, iron and zinc in rice fractions. *Food Chemistry* **2009**, *115* (3), 789-794.
 27. Graf, E., Calcium binding to phytic acid. *Journal of Agricultural and Food Chemistry* **1983**, *31* (4), 851-855.
 28. Dendougui, F.; Schwedt, G., In vitro analysis of binding capacities of calcium to phytic acid in different food samples. *European Food Research and Technology* **2004**, *219* (4), 409-415.
 29. Caldwell, R. A., Effect of calcium and phytic acid on the activation of trypsinogen and the stability of trypsin. *Journal of Agricultural and Food Chemistry* **1992**, *40* (1), 43-46.
 30. Amjad, Z. Inhibition of alkaline earth sulfate scales. US Patent 4,652,377, 1987.
 31. Xu, A.-W.; Yu, Q.; Dong, W.-F.; Antonietti, M.; Cölfen, H., Stable Amorphous CaCO₃ Microparticles with Hollow Spherical Superstructures Stabilized by Phytic Acid. **2005**, *17* (18), 2217-2221.
 32. Koutsoukos, P. G.; Amjad, Z.; Nancollas, G. H., The influence of phytate and phosphonate on the crystal growth of fluorapatite and hydroxyapatite. *Journal of Colloid and Interface Science* **1981**, *83* (2), 599-605.
 33. Grases, F.; Costa-Bauzá, A.; Kroupa, M., Studies on calcium oxalate monohydrate crystallization: influence of inhibitors. *Urological Research* **1994**, *22* (1), 39-43.
 34. F. Grases, R. G.-G. J. J. T. A. L., Effects of Phytic Acid on Renal Stone Formation in Rats. *Scandinavian Journal of Urology and Nephrology* **1998**, *32* (4), 261-265.
 35. Celi, L.; Lamacchia, S.; Barberis, E., Interaction of inositol phosphate with calcite. *Nutrient Cycling in Agroecosystems* **2000**, *57* (3), 271-277.
 36. Amjad, Z., Constant composition study of crystal growth of calcium fluoride. Influence of poly(carboxylic acids), polyphosphates, phosphonates, and phytate. *Langmuir* **1991**, *7* (3), 600-603.
 37. Daneluti, A. L. M.; Matos, J. R., Study of thermal behavior of phytic acid. *Barzilian Journal of Pharmaceutical Sciences* **2013**, *49* (2), 275-283.
 38. Tomson, M. B.; Kan, A. T.; Oddo, J. E., Acid/Base and Metal Complex Solution Chemistry of the Polyphosphonate DTPMP versus Temperature and Ionic Strength. *Langmuir* **1994**, *10* (5), 1442-1449.
 39. Shaw, S. S.; Sorbie, K. S. In *The Effect of pH on Static Barium Sulphate Inhibition Efficiency and Minimum Inhibitor Concentration of Generic Scale Inhibitors*, SPE International Conference on Oilfield Scale, **2012**.
 40. Al Hamad, M.; Al-Sobhi, S. A.; Onawole, A. T.; Hussein, I. A.; Khraisheh, M., Density-Functional Theory Investigation of Barite Scale Inhibition Using Phosphonate and Carboxyl-Based Inhibitors. *ACS Omega* **2020**, *5* (51), 33323-33328.
 41. Bieth, H.; Spiess, B., A comparative study of the protonation of myo-inositol hexakis(phosphate). *Journal of the Chemical Society, Faraday Transactions 1: Physical Chemistry in Condensed Phases* **1986**, *82* (6), 1935-1943.
 42. Vekilov, P. G., The two-step mechanism of nucleation of crystals in solution. *Nanoscale* **2010**, *2* (11), 2346-2357.
 43. Vekilov, P. G., Dense Liquid Precursor for the Nucleation of Ordered Solid Phases from Solution. *Crystal Growth & Design* **2004**, *4* (4), 671-685.

44. Gebauer, D.; Kellermeier, M.; Gale, J. D.; Bergström, L.; Cölfen, H., Pre-nucleation clusters as solute precursors in crystallisation. *Chemical Society Reviews* **2014**, *43* (7), 2348-2371.
45. Erdemir, D.; Lee, A. Y.; Myerson, A. S., Nucleation of Crystals from Solution: Classical and Two-Step Models. *Accounts of Chemical Research* **2009**, *42* (5), 621-629.
46. Ruiz-Agudo, C.; Ruiz-Agudo, E.; Putnis, C. V.; Putnis, A., Mechanistic Principles of Barite Formation: From Nanoparticles to Micron-Sized Crystals. *Crystal Growth & Design* **2015**, *15* (8), 3724-3733.
47. Ruiz-Agudo, C.; Ruiz-Agudo, E.; Burgos-Cara, A.; Putnis, C. V.; Ibáñez-Velasco, A.; Rodríguez-Navarro, C.; Putnis, A., Exploring the effect of poly(acrylic acid) on pre- and post-nucleation BaSO₄ species: new insights into the mechanisms of crystallization control by polyelectrolytes. *CrystEngComm* **2016**, *18* (16), 2830-2842.
48. Safari, M. S.; Wang, Z.; Taylor, K.; Kolomeisky, A. B.; Conrad, J. C.; Vekilov, P. G., Anomalous Dense Liquid Condensates Host the Nucleation of Tumor Suppressor p53 Fibrils. *iScience* **2019**, *12*, 342-355.
49. Li, Y.; Lubchenko, V.; Vekilov, P. G., The use of dynamic light scattering and Brownian microscopy to characterize protein aggregation. *Review of Scientific Instruments* **2011**, *82* (5), 053106.
50. De Yoreo, J. J.; Vekilov, P. G., Principles of Crystal Nucleation and Growth. *Reviews in Mineralogy and Geochemistry* **2003**, *54* (1), 57-93.
51. Geng, X.; Sosa, R. D.; Reynolds, M. A.; Conrad, J. C.; Rimer, J. D., Alginate as a green inhibitor of barite nucleation and crystal growth. *Molecular Systems Design & Engineering* **2021**, DOI: 10.1039/D1ME00010A.
52. Sosa, R. D.; Geng, X.; Reynolds, M. A.; Rimer, J. D.; Conrad, J. C., A microfluidic approach for probing hydrodynamic effects in barite scale formation. *Lab on a Chip* **2019**, *19* (9), 1534-1544.
53. Poloni, L. N.; Ward, M. D., The Materials Science of Pathological Crystals. *Chemistry of Materials* **2014**, *26* (1), 477-495.
54. Cabrera, N.; Vermilyea, D.; Doremus, R.; Roberts, B.; Turnbull, D., Growth and perfection of crystals. **1958**, 393.